Highly efficient metal–organic frameworks for removal of industrial dyes from aqueous solutions

Mohamed A. El-Bindary[a,*], Ahmed Shahat[b], Ibrahim M. El-Deen[c], Muhammad A. Khalil[c], Nader Hassan[c]

[a]Basic Science Department, Higher Institute of Engineering and Technology, New Damietta 34517, Egypt,
Tel. +20 1164126591; Fax: +20 572433265; email: m.a_bindary@yahoo.com
[b]Chemistry Department, Faculty of Science, Suez University, Suez 43518, Egypt
[c]Chemistry Department, Faculty of Science, Port Said University, Port Said 42511, Egypt

ABSTRACT

Metal-organic frameworks (MOFs) are particularly interesting within the adsorption of organic contaminants. This research investigated the adsorption of acid red 57 (AR57) and methylene blue (MB) in aqueous medium using NH_2-MIL-101(Cr) as adsorbent. MOF were described by X-ray diffraction (XRD), N_2 adsorption-desorption (BET), Scanning Electron Microscopy (SEM) and Fourier transform infrared spectroscopy (FTIR). The fabricated MOF has 1467.75 m^2/g huge surface area and pore volume 2.15 cm^3/g which classified as mesopores. NH_2-MIL-101(Cr) demonstrated high adsorption capacity are 953.90 and 553.75 mg/g for AR57 and MB, individually. The Langmuir isotherm was discovered as a good fitting for the laboratory results. A pseudo-second-order rate look was used to describe the mechanism of dye absorption. Similarly, the adsorption activation energy remained discovered being 48.71 and 15.91 kJ/mol for AR57 and MB respectively, implying that adsorption mode is chemisorption. Thermodynamic limits like $\Delta G°$, $\Delta H°$, and $\Delta S°$ were calculated at a variety of temperatures.

Keywords: Adsorption; NH_2-MIL-101(Cr); Kinetics; Thermodynamics; Isotherm

1. Introduction

The coloring business is one of the biggest and also most significant in the world. Nevertheless, due to the range of colours found in its wastewater, it is seen to be a detrimental source of contamination for wildlife [1]. Mutagenic and carcinogenic of some dyes have been proved. Dysfunction of central nervous system, reproductive system, kidney, liver and brain are some effects of dyes on human being [2]. Therefore removal of dyes from environmental is of important consideration. Textile sectors are thought to discharge about 100 tons of colourants into waterways each year. Dyes starting a number of chemical sectors have long been thought to be the main constituent of wastewater. Textile companies use more than 700,000 tones of dyes, making them one of the highest three polluters. Most reactive dyes are hazardous, with the possibility of causing teratogenic and cancerous alterations [3]. For its greater effectiveness, simplicity of use and economic viability, adsorption is regarded a green and environmentally friendly processing technology among the many available [4].

Owing to their colour and the degradation components of the dyes, that are poisonous and harmful to living creatures, dye effluent should not be discharged into water. With regard to their physicochemical characteristics of heat/light opposition, non-biodegradability, and the accumulation of toxic organic groups (such as azo, anthraquinone, etc.), they interrupt the photosynthetic

* Corresponding author.

activity while simultaneously enhancing the biological oxygen demand, chemical oxygen demand, total suspended solids and total dissolved solids, endangering the natural equilibrium and endangering the health of various living things [5]. Additionally, they exhibit teratogenic, mutagenic, carcinogenic and immunogenic characteristics even at low doses, which leads to a physiologic and genetic conundrum of allergy issues, harm to the central nervous and reproductive systems, genetic disorder, besides renal malfunction [6].

Dyes show a significant part in the fabric, pigment and paint industries today, with at least 100,000 distinct dye categories widely accessible. It is believed that 1.6 million tones of dyes are created aimed at meeting industrial demand, with 10%–15% of this volume wasted as wastewater [7]. By means of a consequence, dyes are significant polluters of the environment. Excessive dye exposure causes skin irritation, respiratory difficulties, and, in the case of certain colours, an increased risk of cancer in humans [8]. Furthermore, the existence of dyes in sewerage adds to a high chemical oxidation requirement as well as a foul odour [9]. To ensure the safe disposal of cleaned fluid effluent into watercourses, this is critical to eliminate colourants as quickly as possible from wastewater [10].

Metal–organic frameworks (MOFs) have risen to prominence as a rising star of porous materials in the areas of adsorption and separation, because of their high porosity and specific surface area, as well as their customizable structure and function. Many publications on the manufacturing and usage of MOFs have recently been published. A few publications related to the formation of mesoporous MOFs and their potential uses [11], while the others looked at the effectiveness of MOFs in removing various contaminants, such as heavy metal contamination [12], radioactive and toxic metal ions, aromatic contaminants [13] and azo dye. Additional studies looked at the mechanics of adsorption.

Several MOF resources, containing of a metal-cluster associated by organic molecules as linkers, have been synthesized [14]. Charged MOFs are able to undergo post-synthetic modification by ion exchange, so the MOFs charge (cationic, anionic, or neutral) greatly affects their performance. Recently, porous MOFs with the ability of separation and absorption toward pollutants have been applied in several fields such as water treatment, inclusion of large biomolecules, and capturing harmful dyes [15]. Still, few MOFs have been utilized to remove dye molecules [16]. As a result, creating porous MOFs to filter out ions or big macromolecules remains difficult.

With both the rise in global demographic and, as a result, increased product demand, industrial activity have increased significantly recently [17]. Consequently, the amount of wastewater produced has risen [18]. These waterways could have a high concentration of contaminants, like as dyes. Unsuitable treatment of these wastewaters can jeopardise the integrity of the aquatic organizations that serve as receivers aimed at their outflow, resulting in water environmental contamination concerns for the entire ecosystems that are affected [19]. Adsorption is an efficient dye removal technology owing to its poor operating cost and high maximum removal, particularly when suitable adsorbents are used [20]. Nano-adsorbents, in especially,

have been recommended as an efficient separating surface for reducing dye content in aqueous environment [21].

This paper discusses, fabrication of NH_2-MIL-101(Cr) MOF via hydrothermal reaction for simultaneous adsorption of AR57 and MB molecules. Amino functional MOFs are found to be ideal supports and absorbent materials owing to the advantages of high hydrothermal stability, high specific surface area and post-process modification of amino performance. The resulting NH_2-MIL-101(Cr) was described by FT-IR, XRD, SEM and EBT. The NH_2-MIL-101(Cr) adsorption conditions, like as the time, pH and the initial dye concentrations, have been improved, and the adsorption of kinetics and thermodynamics were investigated. Additionally, the dynamic adsorption and adsorption reusability achievements were assessed.

2. Resources and techniques

2.1. Substances

2-Aminoterephthalic acid (99%), chromium(III) nitrate ($Cr(NO_3)_3$·$9H_2O$), hydrochloric acid, sodium hydroxide, N,N-dimethyl-formamide (DMF), acid red 57 (AR57), methylene blue (MB) were acquired from Alfa Aesar, Anhydrous ethanol, methanol, acetone from Sinopharm Co., Ltd. supplied them. All solutions were diluted with deionized (DI) water. The chemicals included in this research were existed in local markets with analytical grade and utilised with no additional purification.

2.2. NH_2-MIL-101(Cr) preparation

NH_2-MIL-101(Cr) was carried out in compliance with an earlier studies, with certain adjustments [22]. In brief, 1.50 g of chromium (III) nitrate nonahydrate and 0.69 g of 2-aminoterephthalic acid were diffused in deionized water 25 mL, and was instantly heated at 130°C in a 150 mL autoclave for 24 h. Following the completion of the reaction, the resulting green powder was washed thoroughly many times at room temperature to get rid of any remaining 2-aminoterephthalic acid. Eventually, NH_2-MIL-101(Cr) was gained through dipping the powder in dimethyl ketone for 6 h, followed by 4 h of drying at 60°C.

2.3. Making the dyes solutions

1.0 g/L of AR57 and MB dyes were prepared by adding a certin amount of dyes then completing to desired concentration [23]. The stock solution was first diluted successively with deionized water, and after that, the practical concentrations being made. Prior combining with the NH_2-MIL-101(Cr), we use 0.10 M solutions of HCl and NaOH to correct the initial pH of each test. Table 1 shows AR57 and MB features and molecular structure [24].

2.4. Characterization of NH_2-MIL-101(Cr)

All the apparatus used are discussed previously [25,26].

2.5. Batch adsorption studies using experimental design

Batch adsorption investigations were conducted in a variety of settings with AR57 and MB as the adsorption aims

to calculate the adsorption activity of NH_2-MIL-101 (Cr). In a typical procedure, 0.01–0.10 g of NH_2-MIL-101(Cr) was dissolved per 25 mL of AR57 and MB solutions by dissimilar initial concentrations under a certain pH value (0.10 M HCl or 0.10 M NaOH for pH regulating), then the solutions were stirred for a set period of time. The concentrations of AR57 and MB were calculated employing UV-Vis spectra at definite intervals by measuring the absorbance at 510 nm and 630 nm, in both. Eq. (1) determines the adsorption capacity (q_e, mmol/g) and Eq. (2) removal efficiency (%):

$$q_e = \frac{(C_i - C_e)V}{m} \tag{1}$$

$$A = \frac{(C_i - C_e)}{C_i} \times 100\% \tag{2}$$

where C_i (mmol/L) is the original concentrations and C_e (mmol/L) is the final concentrations of dyes; V (L) is the volume of AR57 and MB solutions, and M (g) is the mass of sorbent in the flask [27].

3. Results and discussion

3.1. Analysis of NH_2-MIL-101(Cr)

3.1.1. X-ray diffraction pattern

Fig. 1 represents X-ray powder diffraction (XRD) pattern of NH_2-MIL-101(Cr) [28]. The NH_2-MIL-101(Cr) diffraction peaks agreed well with those previously reported, implying effective development of NH_2-MIL-101(Cr) [29].

3.1.2. Analysis of the Fourier-transform infrared

The effective synthesis of NH_2- MIL-101(Cr) has stayed using FTIR. Fig. 2 shows the FTIR spectra of the samples. The extensive peak at 3,394 cm^{-1} is linked to O–H stretching modes of surface water that has been adsorbed [30].

The benzene ring's C=C is owing to the faint peak at 1,571 cm^{-1}. The carboxylic acid groups O–C–O symmetric vibration causes the 1,390 cm^{-1} band, which confirms the attendance of terephthalic acid molecules in the crystal lattice. The benzene ring C–H deformation vibration is responsible for other 1,100; 1,010; 884, and 768 cm^{-1} vibrations. The faint bands of 700–400 cm^{-1} are caused by the COO$^-$ groups entering and exiting bending phases. In both cases, the descriptive identifying bands at 1,625 and 1,264 cm^{-1} were discovered in connection to the bending of the N–H and C–N stretching phases of amines [31,32]. The FTIR spectrum of NH_2- MIL-101(Cr) after AR57 and MB dyes adsorption are shown in Fig. 2. Some bands have been rised to higher wavenumbers, demonstrating connections involving NH_2-MIL-101(Cr) adsorption functional groups following AR57 and MB dye molecules placed on the interface of the NH_2-MIL-101(Cr).
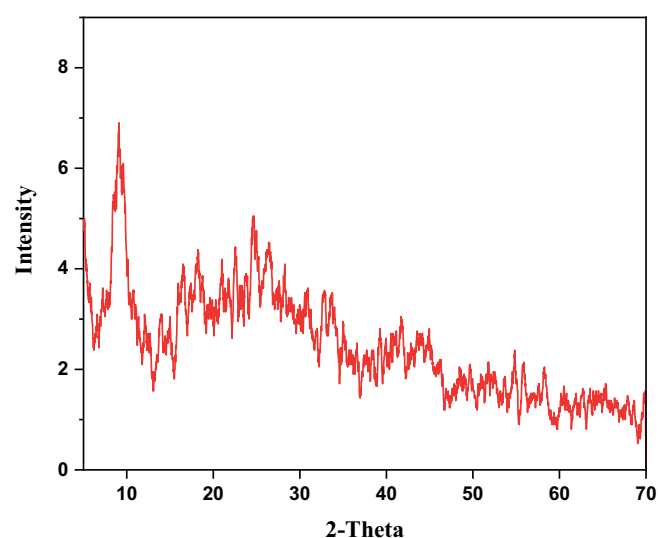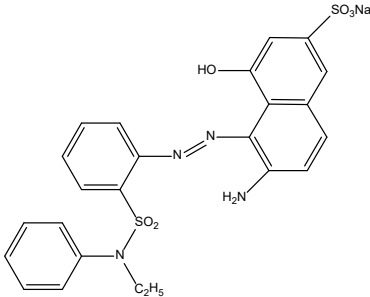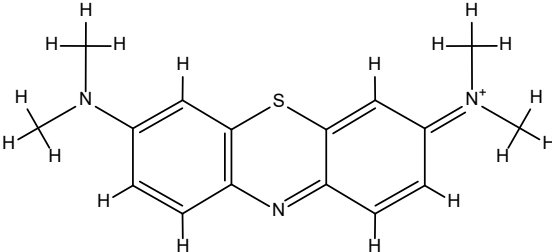

Fig. 1. X-ray diffraction pattern of NH_2-MIL-101(Cr).

Table 1
AR57 and MB features and molecular structure

Chemical formula	$C_{24}H_{21}N_4NaO_6S_2$	$C_{16}H_{18}ClN_3S$
Abbreviation	AR57	MB
Type	Anionic	Cationic
λ_{max} (nm)	510	630
Molecular weight	548.12 g/mol	319.85 g/mol
Molecular formula		
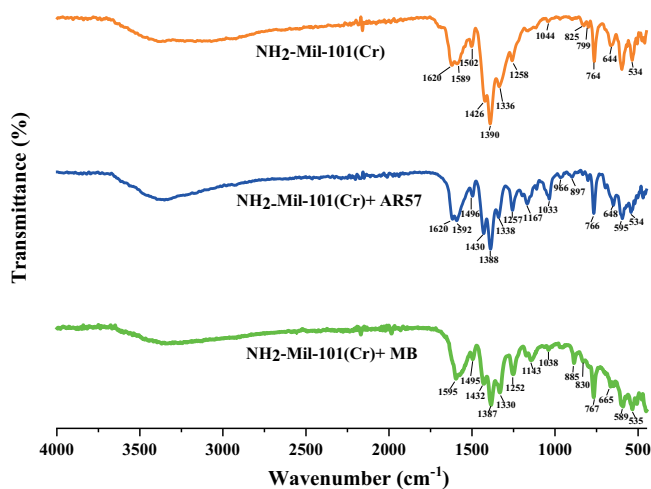
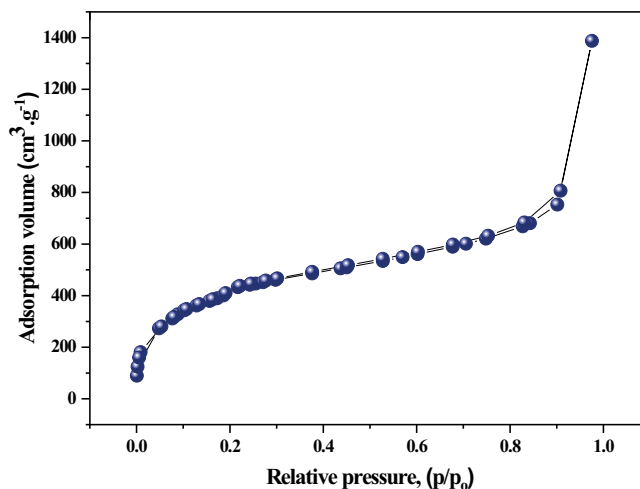Fig. 2. FTIR spectra of NH$_2$-MIL-101(Cr), NH$_2$-MIL-101(Cr)+AR57 and NH$_2$-MIL-101(Cr)+MB.

Fig. 3. NH$_2$-MIL-101(Cr) N$_2$ sorption isotherm.

3.1.3. Analysis of Brunauer–Emmett–Teller (BET)

Fig. 3 illustrates the nitrogen adsorption-desorption isotherms of NH$_2$-MIL-101(Cr). According to IUPAC classification, NH$_2$-MIL-101(Cr) displays type I isotherms, implying that the sample contains mostly micropores. However, a little unclear hysteresis loop was noticed, that is connected by capillary condensation happening in a limited percentage of mesopores, suggesting the presence of a small number of mesopores [33]. It was detected at high relative pressures, a hysteresis loop (P/P_0 > 0.95). NH$_2$-MIL-101(Cr) sample has a BET surface area of 1467.75 m^2/g, as well as a pore volume of 2.15 cm^3/g and a pore size of 2.90 nm. A remarkable decreases in NH$_2$-MIL-101(Cr) surface area was demonstrated after adsorption [32].

3.1.4. SEM analysis

SEM images of the created NH$_2$-MIL-101(Cr) particles are presented in Fig. 4. At the micro scale, produced MOF particles were discovered to be light green powder and exhibited as a polyhedron with uniform particle size [34]. The average diameter of nanoparticles measured was ~68.50 nm as exposed in Fig. 5. Because of NH$_2$-MIL-101(Cr) pores are huge, they have a strong probability of holding and adsorption of dye [35].

3.2. Process experiments

3.2.1. Point of zero charge measurement (pH$_{PZC}$)

NH$_2$-MIL-101(Cr), the point of zero charge (pH$_{PZC}$) stayed strongminded being about pH 7.70, and the positive potentials were observed in the range of 2–7.70, while negative potentials were obtained within the pH values ranging from 7.70 to 12 as shown in Fig. 6 [27].

3.2.2. Effect of pH

The adsorption mechanism is sensitive to the pH of the solution. Dye and adsorbent functional groups seems
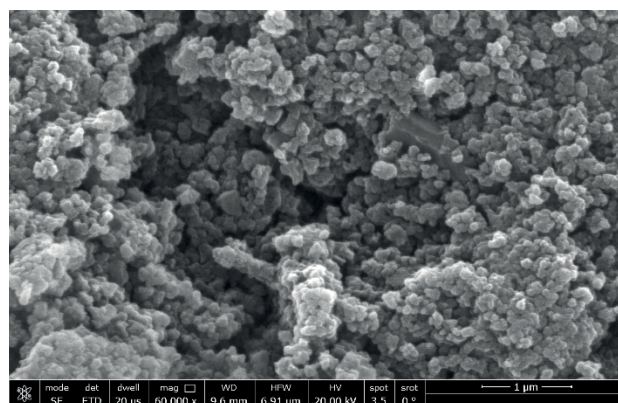

Fig. 4. SEM image of NH$_2$-MIL-101(Cr).

to be disrupted in their solution chemistry. The pH of the solution influences the dye's adsorption performance [36]. Therefore, to additional examine the character of pH during the procedure of adsorption, the adsorption experiments were performed at ambient temperature using AR57 and MB solutions (25 mL, 1.22 × 10^{-3} mmol/L) and (25 mL, 1.06 × 10^{-3} mmol/L) through pH ranging from 2 to 12, respectively. As exposed in Fig. 7, an excellent absorption capacity for AR57 was revealed at pH 3 while pH was 9 for MB and it was used in further studies [37]. The following is a possible explanation for this concept: The percentage of anionic dye removed after solution rises at low pH levels owing to electrostatic interaction among the positive surface charge of the adsorbent and the anionic dye [38]. When the solution has a high pH (basic), there is an electrostatic attraction among the negatively charged adsorbent and the positively charged dye molecule, subsequent in a decrease in the elimination efficiency of anionic dye [39,40]. Whenever the pH level is significant, there are electrostatic attractions between both the positive charges on the dye as well as the negative surface of the sorbents, raising the adsorption capability and withdrawal of cationic dyes
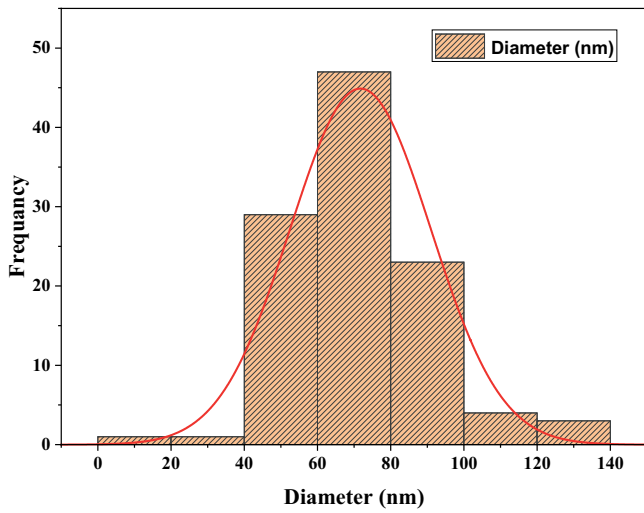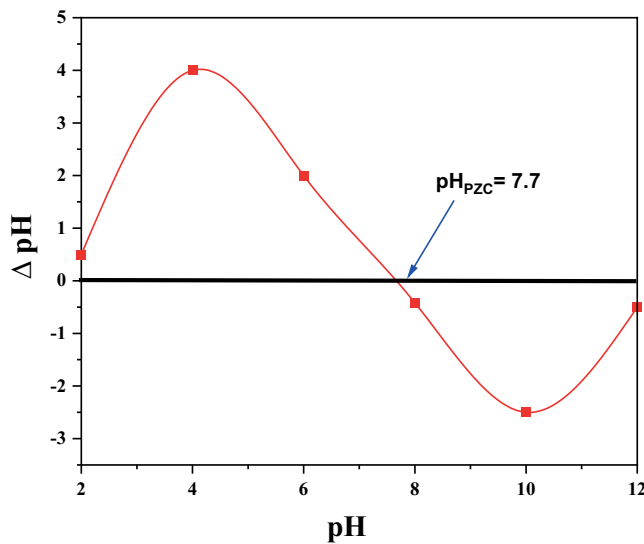
Fig. 5. Average diameter of NH$_2$-MIL-101(Cr).

Fig. 6. Relationship among the original pH besides ∆pH of NH$_2$-MIL-101(Cr).

because the positive charges just on dye ensure that they have been attracted by anionic adsorbent [41,42].

3.2.3. Impact of initial concentration of the dye

Another critical factor in the adsorption procedure is dye concentration. The preliminary concentration can have a major impact on dye elimination by influencing the adsorbent surface's active sites and/or available binding sites [43]. AR57 and MB onto NH$_2$-MIL-101(Cr) was studied through dye concentrations values from 8.85×10^{-4} to 1.90×10^{-3} mmol/L for AR57 while 3.13×10^{-5} to 1.56×10^{-3} mmol/L for MB and NH$_2$-MIL-101(Cr) quantity of 0.02 g. The adsorption effectiveness of AR57 and MB reduced as the original dye concentration increased [44]. Adsorption efficiency is reduced due to the fullness of the active binding sites of NH$_2$-MIL-101(Cr) by increasing concentrations of AR57 and MB.
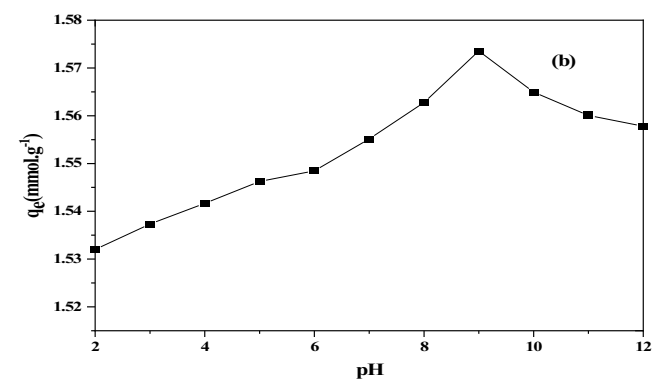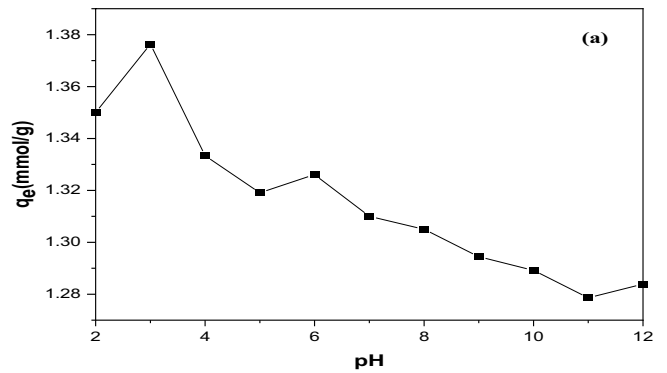

Fig. 7. (a) Influence of pH on AR57 adsorption (T: 25°C; C_i: 1.22×10^{-3} mmol/L) and (b) influence of pH on MB adsorption (T: 25°C; 1.06×10^{-3} mmol/L).

3.2.4. Impact of dosage

Fig. 8 illustrates the adsorption of the dyes AR57 and MB as a purpose of adsorbent dosage. Varying the quantity of NH$_2$-MIL-101(Cr) from 0.01 to 0.10 g/25 mL, by adsorbate concentration 1.22×10^{-3} mmol/L at 25°C and pH 3 for AR57 while for MB concentration 1.06×10^{-3} mmol/L at 25°C and pH 9. The outcomes in Figs. 8a and 9a show the AR57 and MB adsorption strength as a sense of adsorbent quantity. The adsorption efficiency of AR57 and MB was discovered to decrease from 1.38 to 0.34 mmol/g and 1.57 to 0.13 mmol/g, accordingly. Increasing the NH$_2$-MIL-101(Cr) dosage from 0.01 to 0.10 g/25 mL. Figs. 8b and 9b illustrate the impact of quantity on the equilibrium concentration (Ce/C_i) of AR57 and MB by the NH$_2$-MIL-101(Cr) sorbent. By way of the dose increases, the equilibrium concentration of AR57 and MB falls, owing to an increase in the NH$_2$-MIL-101(Cr) surface area [45]. The data exposed assign that the exclusion performance increases up to 92.10% (C_e/C_i = 0.066) at NH$_2$-MIL-101(Cr) dose of 0.10 g/25 mL for AR57, while for MB the removal efficiency rises up to 77.02% (C_e/C_i = 0.229) at NH$_2$-MIL-101(Cr) quantity of 0.10 g/25 mL. It is clear that increasing the NH$_2$-MIL-101(Cr) dose rise the level of adsorbed dye while decreasing adsorption density, or the quantity per unit mass adsorbed [46]. It is clear that enhancing the
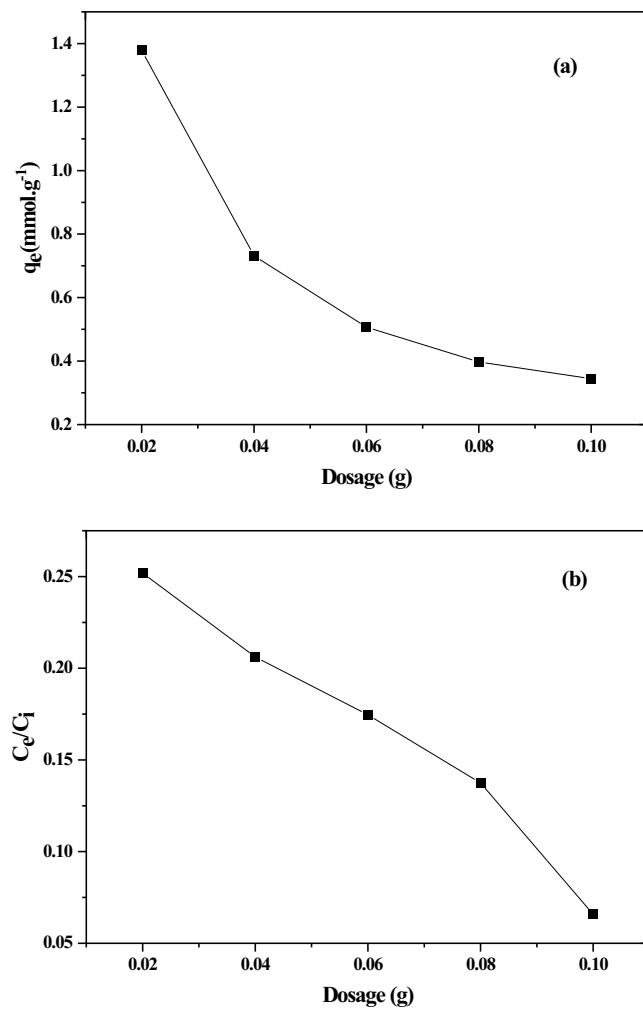
Fig. 8. The influence of NH$_2$-MIL-101(Cr) dosage on the adsorption of AR57: (a) sorption capacity vs. NH$_2$-MIL-101(Cr) dosage and (b) relative remaining concentration (C_e/C_i) vs. NH$_2$-MIL-101(Cr) dosage (C_i: 1.22 × 10^{-3} mmol/L; T: 25.0°C; pH 3.0).

adsorbent dose rises the amount of possible adsorption sites, resulting in a rise in the level of dye adsorbed. The reduction in adsorption density with growing adsorbent quantity is primarily owing to the detail that adsorption sites persist unsaturated through the adsorption operation, so even though expanding the adsorbent dose rises the number of sites obtainable for adsorption [47].

3.3. Adsorption isotherm

Adsorption isotherms remained also utilized to examine the surface features and affinity of adsorbents for objectives. Langmuir [48,49], Freundlich [50], Temkin [51], Dubinin–Radunkevich [51] isotherms were used in this investigation to mathematically characterise the adsorption data in Eqs. (3)–(6):

$$\frac{C_e}{q_e} = \frac{1}{q_m K_L} + \frac{C_e}{q_m} \tag{3}$$
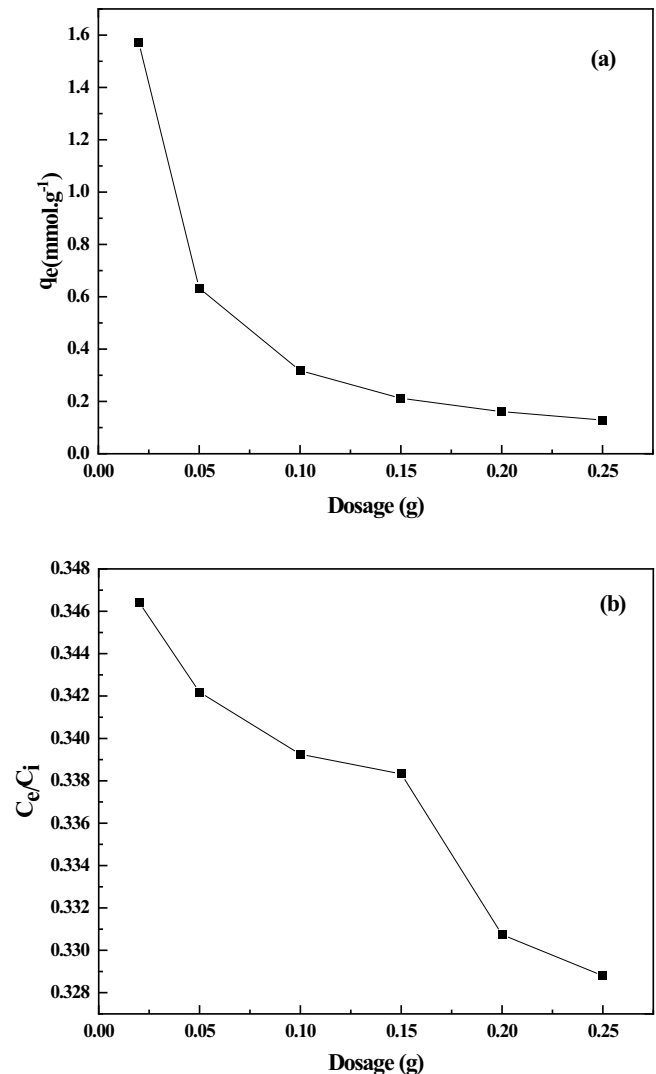
Fig. 9. The influence of NH$_2$-MIL-101(Cr) dosage on the adsorption of MB: (a) sorption capacity vs. NH$_2$-MIL-101(Cr) dosage and (b) relative residual concentration (C_e/C_i) vs. NH$_2$-MIL-101(Cr) dosage (C_i: 1.06 × 10^{-3} mmol/L; T: 25.0°C; pH 9.0).

$$\ln q_e = \ln K_F + \frac{1}{n} \ln C_e \tag{4}$$

$$q_e = \beta_T \ln K_T + \beta_T \ln C_e \tag{5}$$

$$\ln q_e = \ln Q_{DR} - K_{DR} \varepsilon^2 \tag{6}$$

C_e (mmol/L) is the equilibrium concentration of AR57 and MB, and K_L (L/mol) is the Langmuir adsorption constant in these equations. The adsorption capacity of AR57 or MB is q_e (mmol/g), and the predicted ultimate adsorption capacity of NH$_2$-MIL-101(Cr) is q_m (mmol/g). The adsorption equilibrium constants of the Freundlich adsorption isotherm are K_F (mg$^{1-1/n}$ L$^{1/n}$ g^{-1}) and n. The 1/n constant represents distinct types of isotherms: 1/n = 0 suggests irreversible adsorption, 0 < 1/n < 1 implies beneficial

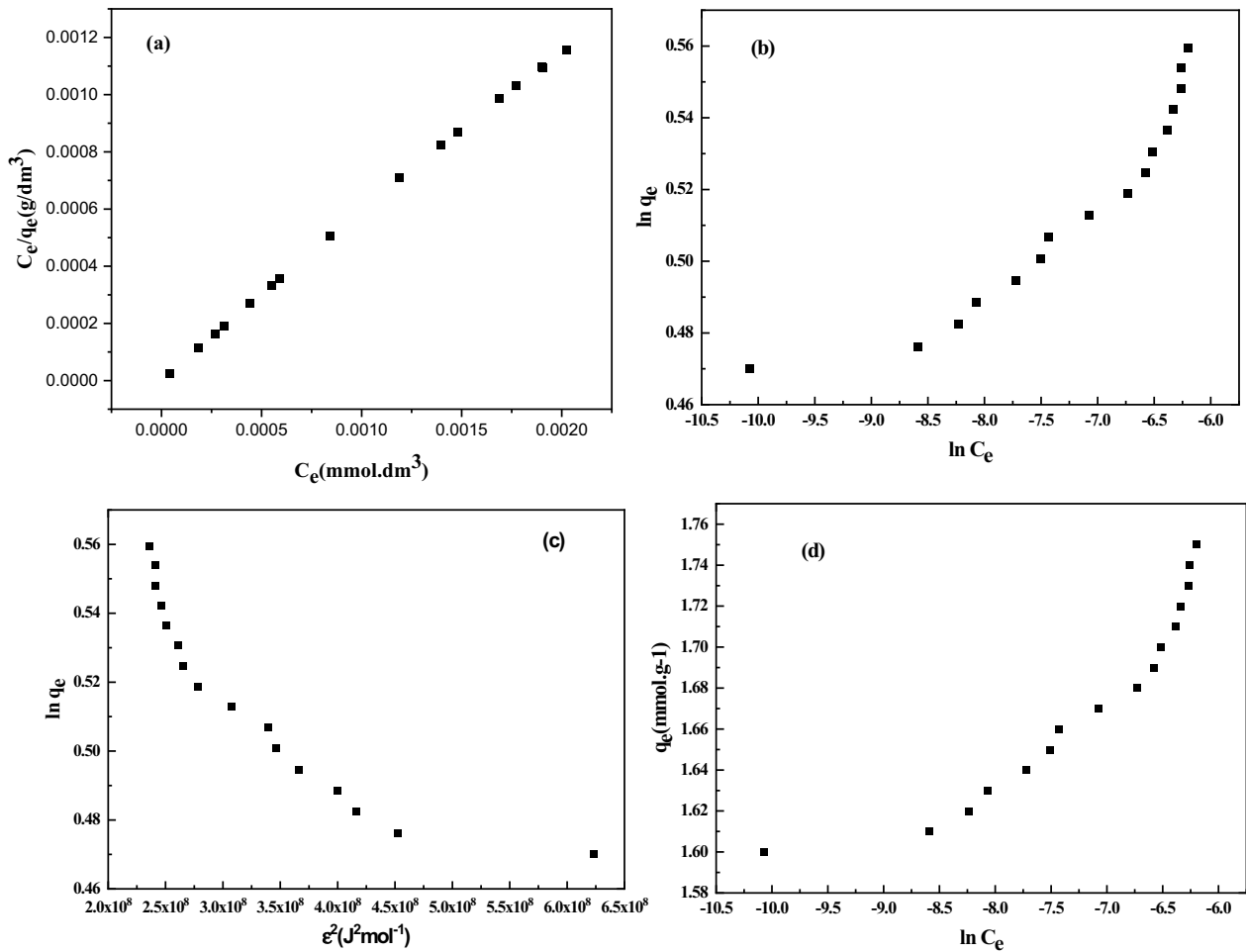Fig. 10. Plots of linearized isothermal AR57 sorption: (a) Langmuir, (b) Freundlich, (c) Dubinin–Radunkevich and (d) Temkin.

adsorption, and $1/n > 1$ demonstrates the reverse. The slope and intercept of the associated linear plot were used to calculate all of the above constants [52,53]. In which equilibrium concentration C_e (mmol/L), amount at equilibrium q_e (mmol/g); maximum adsorption capacity q_m; Langmuir constant K_L (L/mol) and K_F ($\mu g^{1-1/n} mL^{1/n} cm^{-2}$) and n are the Freundlich constants, respectively [54].

Fig. 10 depicts the fitting lines of Langmuir, Freundlich, Temkin, Dubinin–Radunkevich models. Table 2 lists the associated fitting variables of the four models for AR57 and MB. The best combination was chosen nearest of the coefficient of determination (R^2) value to one. Table 2 outlined results of the isotherm modelling [46]. Without a doubt the utmost precise is the Langmuir isotherm model (Figs. 10a and 11a). It designates the attendance of a monolayer adsorption process. AR57 and MB had monolayer adsorption potentials of 1.75 and 1.76 mmol/g (q_m), respectively. The average sorption energy are 48.71 and 15.91 kJ/mol for AR57 and MB, respectively [55]. Regarding the proposed chemisorption process, this is correct. Evidently, the separation limit energy of 8 kJ/mol is commonly believed. Physical sorption (less than 8 kJ/mol) and chemical sorption (up to 8 kJ/mol) [27].

The non-linear expression of Langmuir model is provided in Eq. (7) as implies:

$$q_e = q_m \frac{K_L C_e}{1 + K_L C_e} \tag{7}$$

where q_e and C_e are the quantity of dyes adsorbed at equilibrium (mmol/g) and C_e is the equilibrium concentration (mmol/dm³) [56]. The constants q_m and K_L are assigned to the capacity of adsorption and energy, respectively. The Freundlich isotherm is used to evaluate the multilayer adsorption on a heterogeneous surface. The non-linear form of Freundlich isotherm is illustrated by Eq. (8) as follows:

$$q_e = K_F C_e^{1/n} \tag{8}$$

where K_F and n are the constants given respectively to the adsorption ability and adsorption intensity.

Figs. 10–12 clearly show a saturation plateau reached for residual concentrations close to 1.72 mmol/L. The Freundlich equation being a power-type equation is not appropriate for describing this kind of isotherm shape. On the opposite hand, the Langmuir model supposes that the sorption occurs by monolayer adsorption, without interactions between sorbed molecules and with homogeneous sorption energies
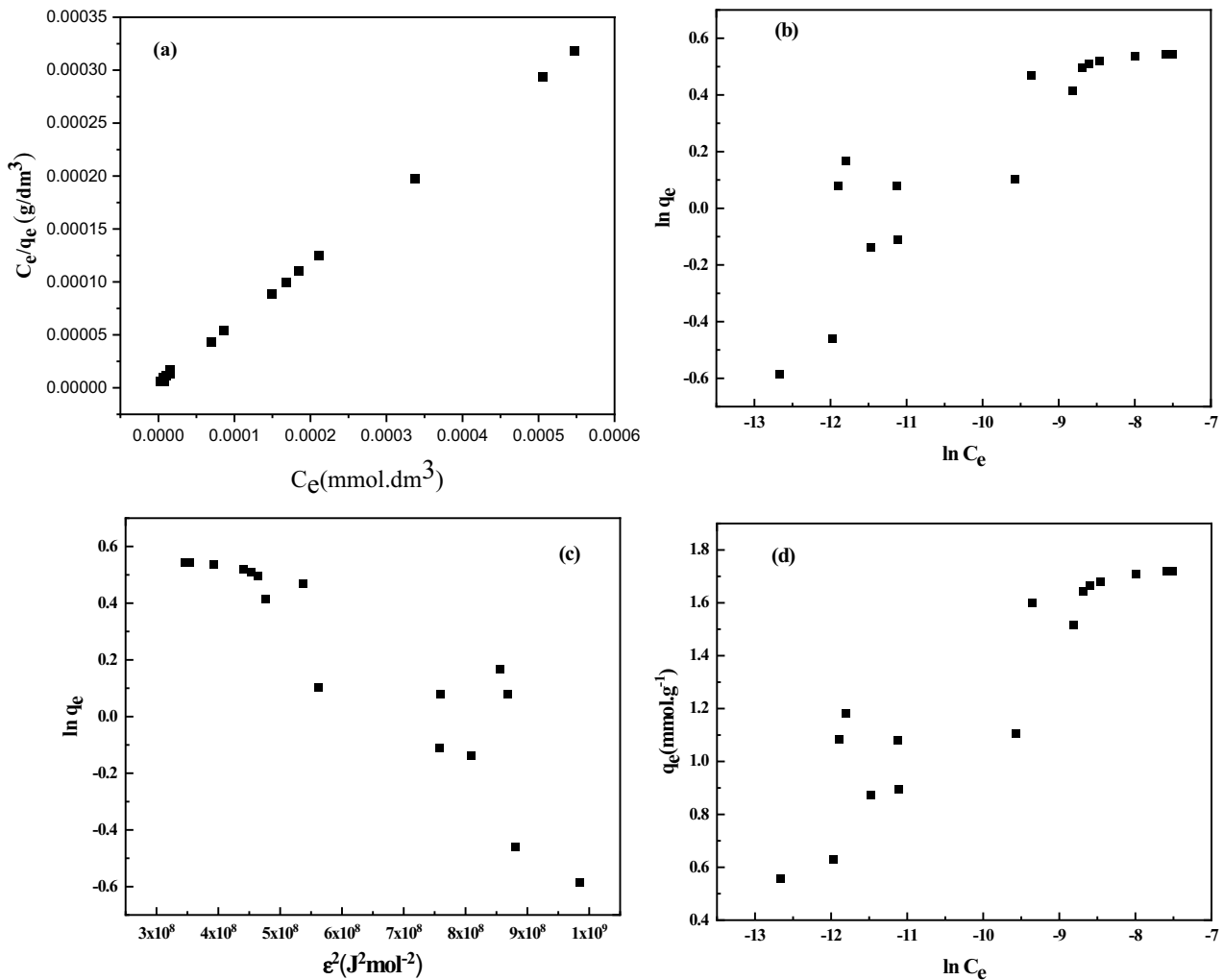
Fig. 11. Plots of linearized isothermal MB sorption: (a) Langmuir, (b) Freundlich, (c) Dubinin–Radunkevich and (d) Temkin.

(including homogeneous distribution of sorption sites at the surface of the sorbent).

Fig. 12 indicates the non-linear adsorption isotherm of (a) AR57 and (b) MB over NH_2-MIL-101 (Cr). It is evident that the adsorption process referred to Langmuir isotherm because of the significance of (R^2) is superior to (R^2) for Freundlich isotherm.

3.4. Adsorption kinetics and mechanism studies

To improvement a better considerate of the progression of kinetic adsorption of AR57 and MB, they were examined by a pseudo-first-order model [57], pseudo-second-order model [58], intraparticle diffusion model and Elovich model [59] that are defined as Eqs. (9)–(12):

$$\log\left(q_e - q_t\right) = \log q_e - \left(\frac{K_1}{2.303}\right)t \tag{9}$$

$$\frac{t}{q_t}\frac{1}{K_2 q_e^2} + \frac{t}{q_e} \tag{10}$$

The sorbent's adsorption efficiency of AR57 and MB at equilibrium and time t (min) are represented by q_e (mmol/g) and q_t (mmol/g), respectively. The pseudo-first-order rate constant K_1 (min^{-1}) and the pseudo-second-order rate constant K_2 (g/mg min) are also represented [Eq. (10)]:

$$q_t = K_i t^{1/2} + X \tag{11}$$

q_t (mmol/g) is the adsorption capacity of the adsorbent by time t (min), the K_i (mg/g min$^{1/2}$) represent the rate constants of intra-particle diffusion by stage i, which is studied from the slope of fitting linear curve q_t vs. $t^{1/2}$, and X is the intercept of stage i [Eqs. (11) and (12)]:

$$q_t = \frac{1}{\beta}\ln\left(\alpha\beta\right) + \frac{1}{\beta}\ln t \tag{12}$$

Fitting curves of pseudo-first-order, pseudo-second-order, intra-particle diffusion and Elovich models are exposed in Figs. 13 and 14 for AR57 and MB respectively. Table 3 shows the correlating kinetic models. Once the appropriate outcomes of these two representations are
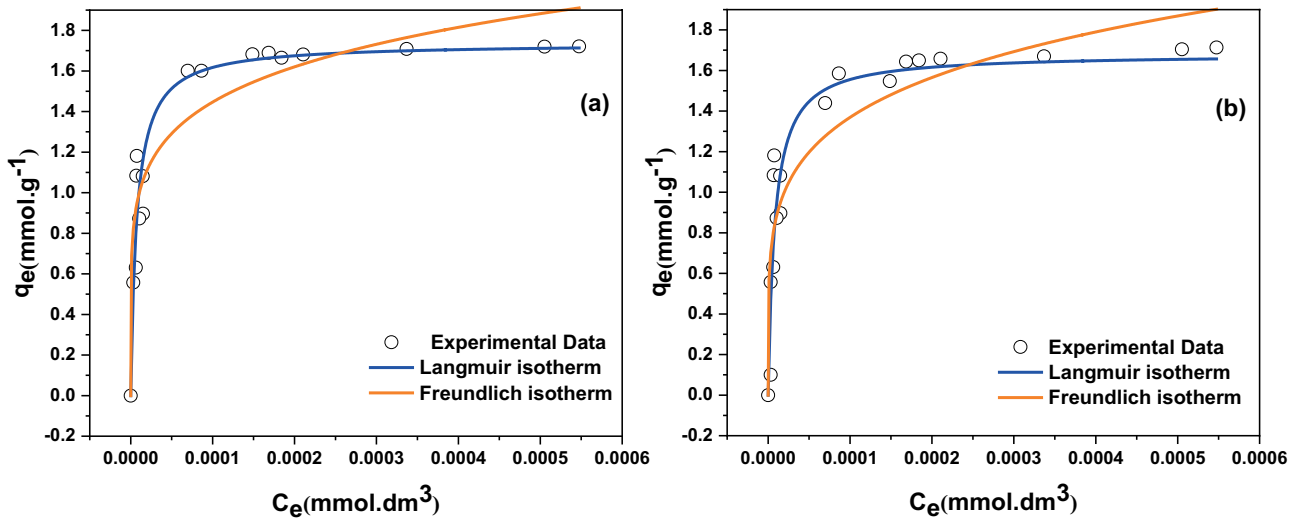
Fig. 12. Non-linear adsorption isotherm of (a) AR57 and (b) MB over NH$_2$-MIL-101(Cr).
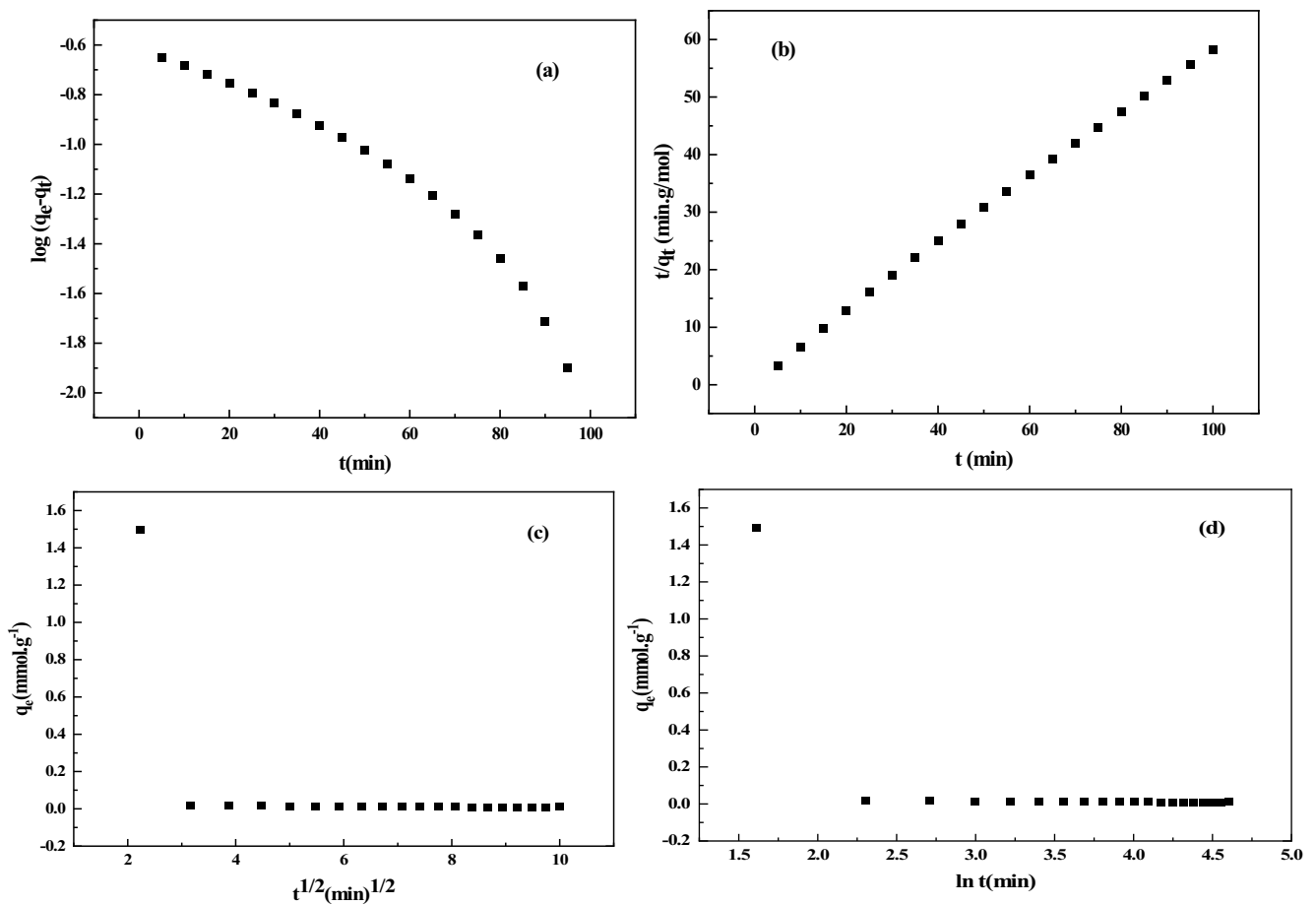
Fig. 13. Plots of linearized isothermal AR57 sorption: (a) pseudo-first-order, (b) pseudo-second-order, (c) intraparticle diffusion and (d) Elovich.

compared, it is evident that the correlation coefficients (R^2) for the pseudo-first-order model (R^2 = 0.938 and 0.898 for AR57 and MB, respectively) are below 0.990, while the R^2 of the pseudo-second-order model is about 0.999 for AR57 and MB, as will the adsorption kinetics of AR57 and MB tend to match the pseudo-second-order model, indicating that chemical adsorption is the primary adsorption procedure among NH$_2$-MIL-101(Cr) and AR57 and MB [60,61].

In the meantime, the high agreement between theoretical and experimental adsorption capacity (q_e) of the pseudo-second-order kinetic model settles the AR57 and MB particles are effectively extracted from aqueous solution through NH_2-MIL-101(Cr), and the adsorption development is influenced through speed of surface response [62,63].

The pseudo-first order [Eq. (13)] and pseudo-second-order [Eq. (14)] equations is given as:

$$q_t = q_e \left(1 - \exp^{-k_1 t}\right) \tag{13}$$

$$q_t = \frac{k_2 q_e^2 t}{1 + k_2 q_e t} \tag{14}$$

where, k_1 (min^{-1}), k_2 (g/mg min^1) are the pseudo-first-order, pseudo-second-order rate constants, respectively [56]. Different kinetics models are shown in Fig. 15.

3.5. Adsorption thermodynamics

A thermodynamic investigation was approved between the temperatures of 298 and 318 K. The percentage of AR57 and MB particles adsorbed by NH_2-MIL-101(Cr) rose as heating increased, from 1.06 to 1.22 mmol/g for AR57 and 1.29 to 1.30 mmol/g for MB, respectively, which could be described through the endothermic nature of the adsorption mechanism, which allows the AR57 and MB molecules to move more freely at elevated temperatures [64]. The thermodynamics variables at equilibrium, such as the standard enthalpy change ($\Delta H°$), standard Gibbs free energy change ($\Delta G°$) and standard entropy change ($\Delta S°$),

were analysed in this examination to define the effects of temperature; these variations are derived from Eqs. (15)–(17):

$$K_c = \frac{q_e}{C_e} \tag{15}$$

$$\Delta G° = -RT \ln K_c \tag{16}$$

$$\ln K_c = \frac{\Delta S°}{R} - \frac{\Delta H°}{RT} \tag{17}$$

where q_e (mmol/g) and C_e (mmol/L), respectively, reflect the adsorption capacity and equilibrium concentration of AR57 and MB. K_c is compatible with the thermodynamic equilibrium constant, and R is the ideal gas constant [65]. The actual temperature is T (K). The slope and intercept of the linear regression of $\ln K_c$ vs. $1/T$, as well as the $\Delta G°$, which represents the change in the standard Gibbs free energy, are used to estimate the values of $\Delta H°$ (kJ/mol) and $\Delta S°$ (J/mol K) (Figs. 16 and 17). Table 4 contains the correlating thermodynamic data that were determined and executed. The negative standards of ΔG and positive standards of ΔS propose the adsorption procedure of AR57 and MB through NH_2-MIL-101(Cr) is spontaneous and satisfactory. Furthermore, as temperature increased, positive ΔH values increased but ΔG values declined, indicating an endothermic reaction at elevated temperatures [66].

Table 2
Variables for various parameter isotherm models for the study of the adsorption of both the dyes AR57 and MB over NH_2-MIL-101(Cr)

Isotherm models	Parameters	AR57 dye	MB dye
Langmuir	$q_{m,exp}$ (mmol/g)	1.750	1.720
	q_m (mmol/g)	1.746	1.757
	K_L (L/mmol)	0.389	125,054.945
	R^2	0.999	0.999
Freundlich	N	41.169	1.223
	K_F (mmol/g) (L/mmol)$^{1/n}$	0.690	7.832
	R^2	0.846	0.774
Dubinin-Radunkevich	Q_{DR}	0.596	1.154
	K_{DR} (J^2/mol^2)	2.43E-10	1.53E-9
	E (kJ/mol)	45.361	18.036
	R^2	0.788	0.797
Temkin	b_T (L/mol)	61,326.040	11,470.241
	A_T (kJ/mol)	48.713	15.912
	R^2	0.839	0.844

Table 3
Adsorption of AR57 and MB dyes on NH_2-MIL-101(Cr) by means of pseudo-first-order, pseudo-second-order, Elovich, besides intraparticle diffusion models, as well as correlation coefficients

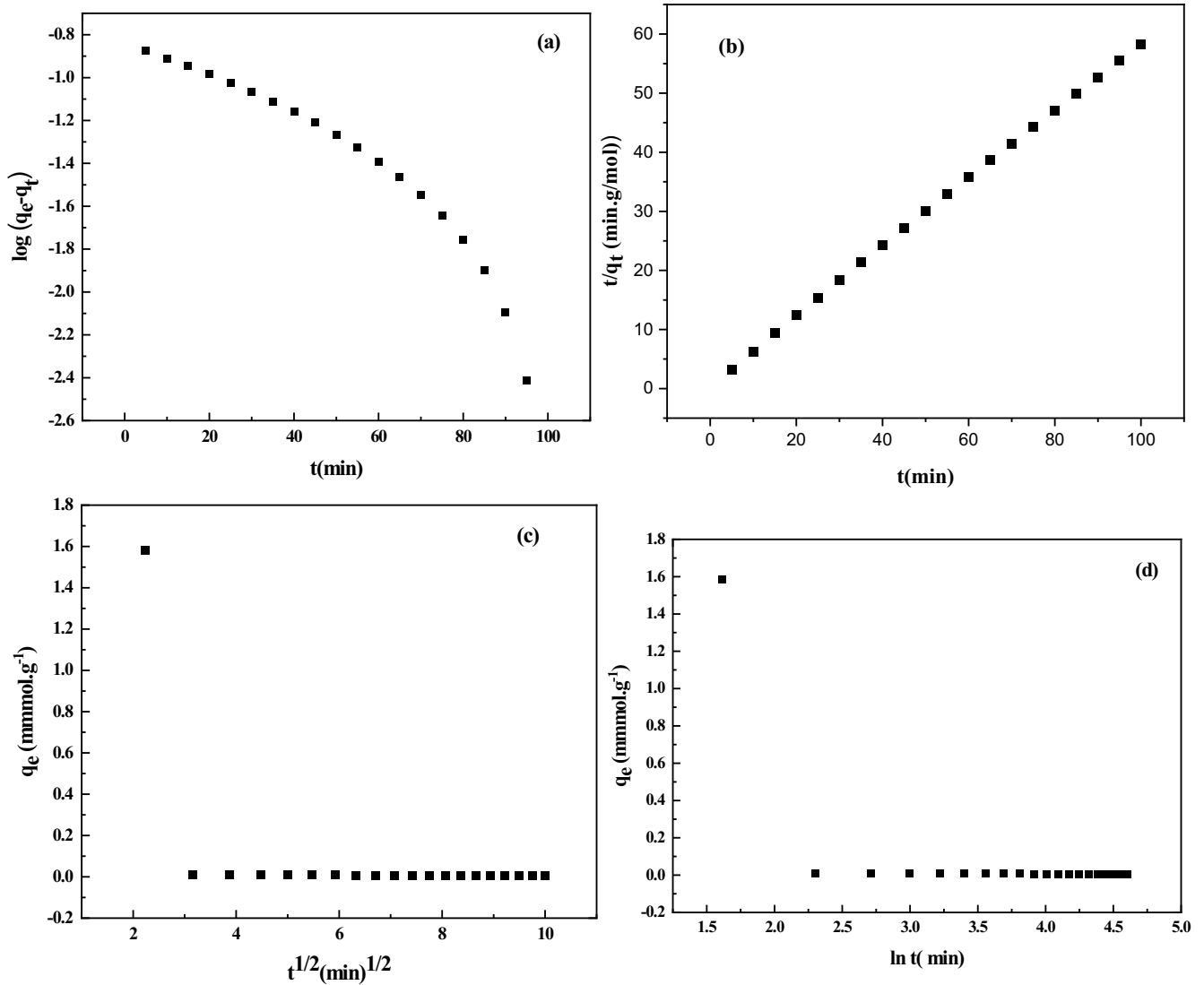| Kinetic model	Dye	Parameters	Value	R^2
Pseudo-first-order model	AR57	q_e (mmol/g)	–0.324	0.938
		k_1 (min^{-1})	–0.0125	
	MB	q_e (mmol/g)	–0.188	0.898
		k_1 (min^{-1})	–0.014	
Pseudo-second-order model	AR57	q_e (mmol/g)	1.739	0.999
		k_2 (g/mg min)	0.217	
	MB	q_e (mmol/g)	1.731	0.999
		k_2 (g/mg min)	0.379	
Elovich	AR57	β (g/mg)	–3.891	0.349
		α (mg/g min)	2.794	
	MB	β (g/mg)	3.745	0.346
		α (mg/g min)	2.955	
Intraparticle diffusion model	AR57	k_i (mg/g min$^{1/2}$)	–0.070	0.195
		X (mg/g)	0.573	
	MB	k_i (mg/g min$^{1/2}$)	–0.747	0.192
		X (mg/g)	0.600	
Experimental data	AR57	q_e(exp) (mmol/g)	1.718	
	MB	q_e(exp) (mmol/g)	1.716	

Fig. 14. Plots of linearized isothermal MB sorption: (a) pseudo-first-order, (b) pseudo-second-order, (c) intraparticle diffusion and (d) Elovich.

Table 4
Thermodynamic functions ΔG, ΔS and ΔH of AR57 and MB adsorbed by NH$_2$-MIL-101(Cr)

Dye	T (K)	T (K)	$\Delta G°$ (kJ/mol)	$\Delta H°$ (kJ/mol)	$\Delta S°$ (J/mol K)
	298		−2.641		
	303		−2.966		
AR57	308	252.277	−3.290	16.360	64.87
	313		−3.614		
	318		−4.263		
	298		−1.274		
	303		−1.653		
MB	308	276.190	−2.032	20.940	75.82
	313		−2.411		
	318		−3.170		

Fig. 15. Non-linear kinetic data of (a) AR57 and (b) MB over NH2-MIL-101 (Cr).

Fig. 16. (a) Van't Hoff plots and (b) Arrhenius plots for AR57 adsorption by NH_2-MIL-101(Cr).

3.6. Effect of ionic strength

As it's well understood that industrial effluents always contain contaminants such as inorganic salts, ionic strength is an vital influence to investigate in adsorption studies. The presence of these salts in solution results in high ionic strength, which affects the entire adsorption procedure [67]. The influence of ionic strength on NH_2-MIL-101(Cr) efficacy against AR57/MB dyes was carefully modeled to confirm the efficacy of NH_2-MIL-101(Cr) in real wastewater cleanup. The purifying of AR57 and MB dyes was significantly reliant on the quantity of other competitive ions existing in the aqueous solution, as seen in Fig. 18. Although, the decrease in loading measurements of NH_2-MIL-101(Cr) through an improvement in the competitor's density (i.e., Cl$^-$), the absorbent still has very high adsorption capabilities of 1.314 mg/g ($R\% = 79.88\%$) and 1.505 mg/g ($R\% = 88.37\%$) for AR57 and MB dyes, respectively. From a broad perspective, the little difference can be elucidated in thi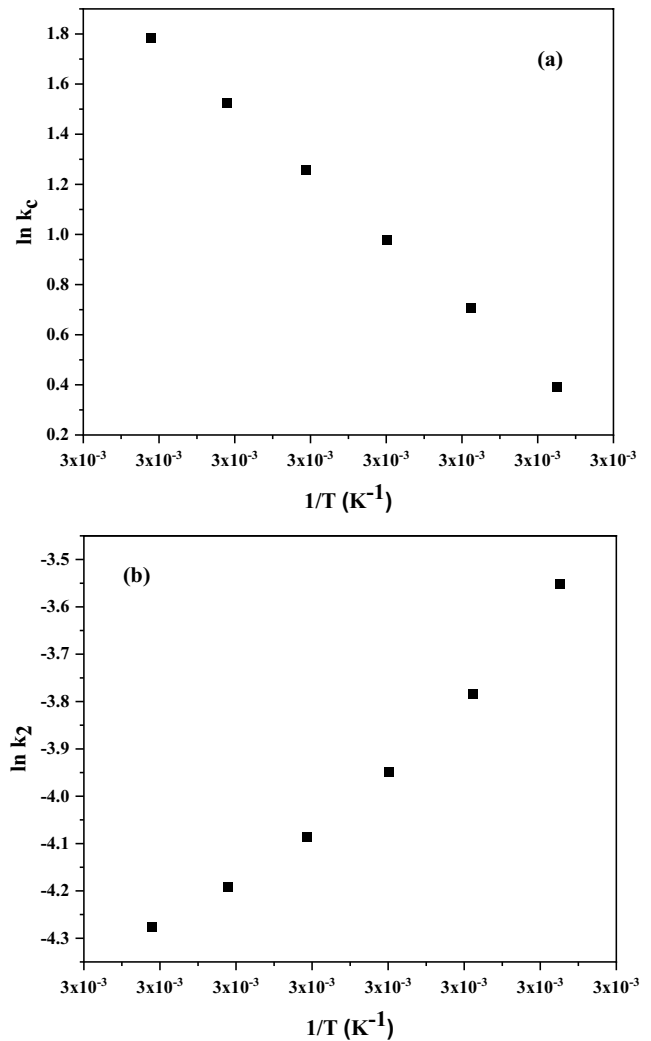s section [68]. The rise in the electrolyte counters ions concentration coated the NH_2-MIL-101(Cr) surface, slowing the adsorption procedure. The double electric layer was also squeezed by an increase in solution salinity, which created an electrostatic repulsion among both the anionic dyes and the adsorbent [69,70]. Other investigations have observed similar antagonistic effects of inorganic contestants by adsorption of organic dyes by means of numerous adsorbents, which is a more accurate assessment [24,71].

3.7. Comparison with other adsorbents

The maximal AR57 and MB adsorption possibilities attained with NH_2-MIL-101(Cr) as just an adsorbent are compared to those attained with another mentioned previously adsorbents in Tables 5 and 6.

3.8. Interactional process

The method of AR57 and MB adsorption upon that NH_2-MIL-101(Cr) surface remained established by means of batch experiments and adsorption isotherms. Hydrophobic
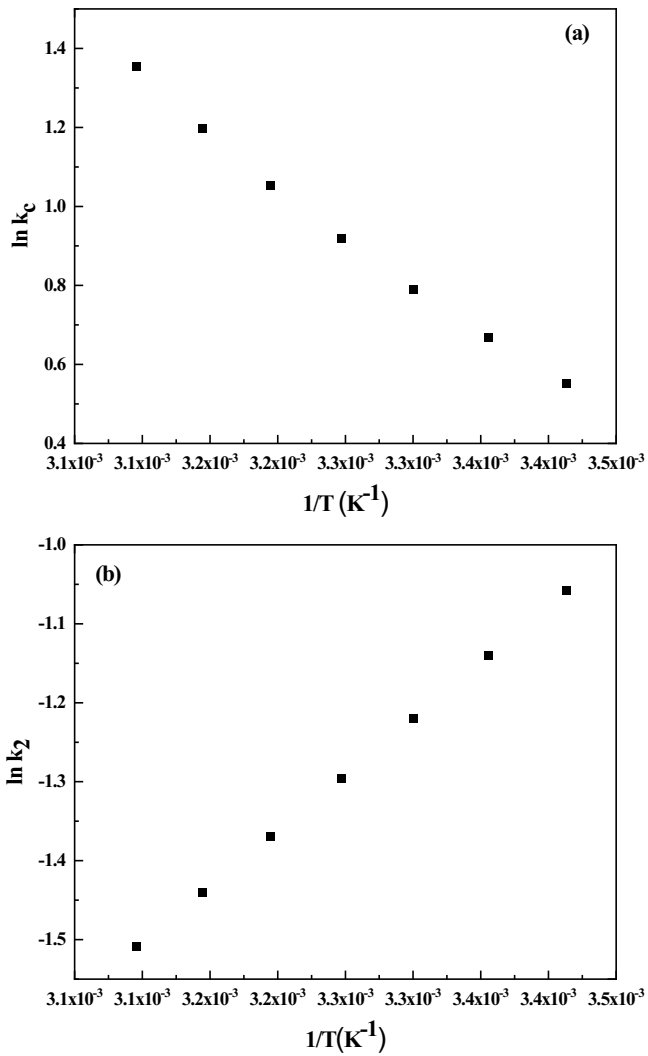
Fig. 17. (a) Van't Hoff plots and (b) Arrhenius plots for MB adsorption by NH_2-MIL-101(Cr).

Table 5
Different adsorbents mentioned in the literature are used in comparative studies of AR57 sorption

Adsorbate	q_m (mg/g)	References
SMS	425	[72]
Sepiolite	134.60	[73]
HTAB-MS	307.40	[74]
AAB	416.30	[75]
MIONS	930.16	[25]
MCCM	1,162.70	[76]
NH_2-MIL-101(Cr)	953.90	This work

reactions and π-π stacking connections could be the major causes of contact among AR57 and MB dyes and NH_2-MIL-101(Cr). Furthermore, van der Waals forces contributed to adsorption. These interactions are all help the AR57 and MB dyes, as well as NH_2-MIL-101(Cr), to adsorb.
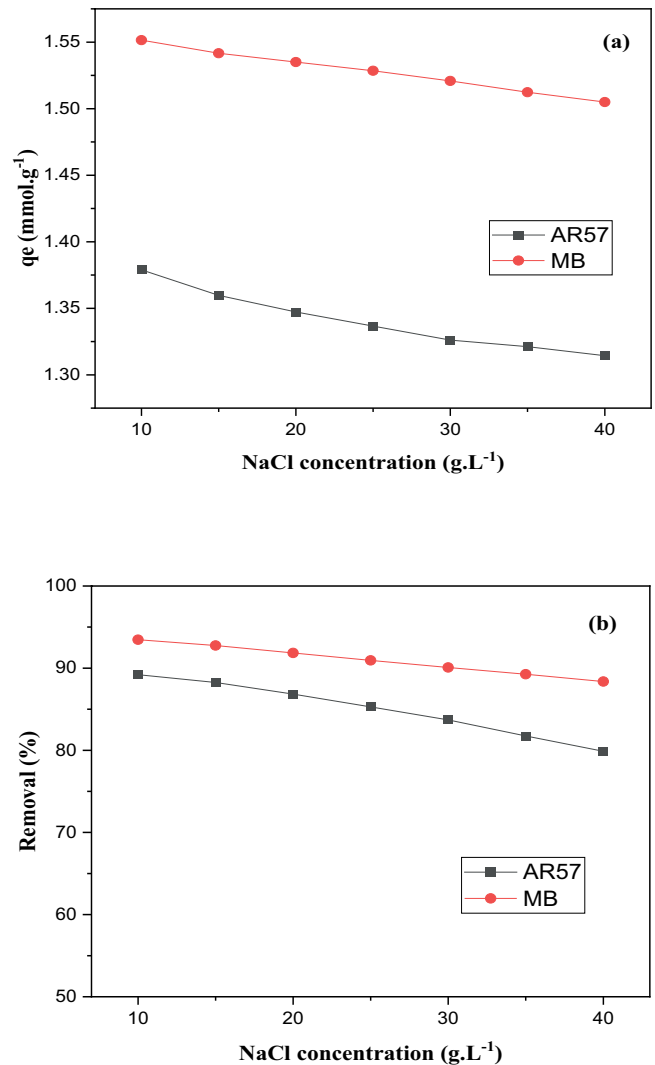
Fig. 18. Effect of NaCl on dyes adsorption onto the NH_2-MIL-101(Cr) adsorbent (a) AR57 (C_i: 1.22 × 10^{-3} mmol/L; initial pH 3.0; T: 25°C; sorbent dosage: 0.02 g/25 mL) and (b) MB (C_i: 1.06 × 10^{-3} mmol/L; initial pH 9.0; T: 25°C; sorbent dosage: 0.02 g/25 mL).

Table 6
Different adsorbents mentioned in the literature are used in comparative studies of MB sorption

Adsorbate	q_m (mg/g)	References
AC (rattan sawdust)	294.14	[77]
OP	20.50	[56]
AOS	22.10	[78]
Fe-BDC MOF	8.65	[79]
Co doped Fe-BDC MOF	23.92	[18]
CH	30.33	[80]
C-BTC	143.27	[80]
HKUST-1/GO	140	[81]
ZIF-8	522.95	[82]
NH_2-MIL-101(Cr)	553.75	This work

Moreover, NH_2-MIL-101(Cr) contains a benzene ring, that could stimulate attraction of mixtures comprising benzene rings via π-π stacking communication [83–85].

By lowering the pH underneath the zero charge threshold, surface charge for NH_2-MIL-101(Cr) develops more positive, facilitating AR57 adsorption on it's own surface. On other hand by increasing the pH above point of zero charge the surface charge of NH_2-MIL-101(Cr) become more negative, leading to attraction between Cr^{3+} with SO_3^- of AR57 and attraction between NH_2 with CH_3 of MB.

3.9. Reactive sites

The reactive areas in the under-review adsorbate/adsorbent organization, in addition the electrophilic/nucleophilic attacking area besides zero electrostatic potential zones, are all determined using the molecular electrostatic potential (MEP) approach [84]. In Fig. 19 molecular electrostatic potentials (MEP) when utilised to visualise the electron density throughout full surface of NH_2-MIL-101(Cr), AR57, and MB. The assessed MEP's results were depicted on these maps with diverse colors (green, red, yellow, blue and light blue). Negative MEP standards are represented by the colors red besides yellow, which are related with an electrophilic attack; positive MEP results are represented by the colors blue and green, which are allied with a nucleophilic attack; and MEP attacks are represented by the green color. The MEP map reveals that NH_2-MIL-101(Cr) adsorbents are most vulnerable to electrophilic attacks, whereas the AR57 and MB adsorbates MEP confirms that nucleophilic attacks are the most common in the adsorbates Fig. 19a and b also depicts nucleophilic besides electrophilic attacks on the AR57, MB, and NH_2-MIL-101(Cr) adsorbent surfaces. The emergence of green hue, owing to the high electrostatic interaction between AR57 beside
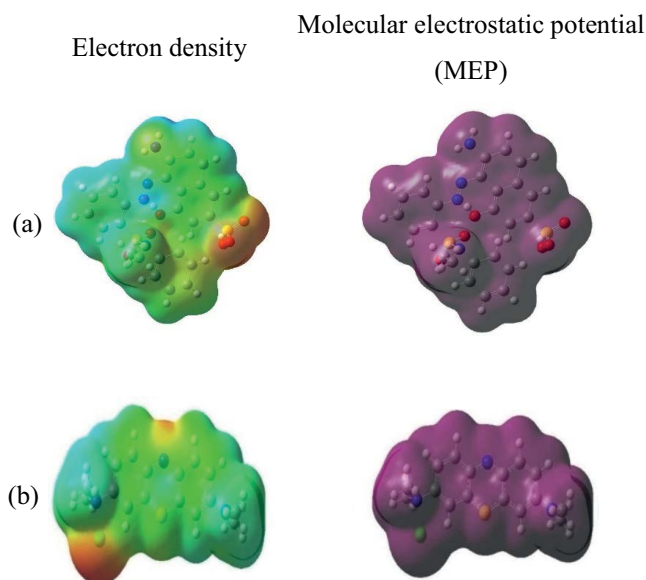
MB with NH_2-MIL-101(Cr), this designates a neutral surface charge, specifies a higher electrostatic interaction among them [85].

3.10. Desorption studies

The used adsorbent should be re-usable from a financial perspective. The saturated active sites proceeding the adsorbent surface need to recharged in order to prepare for further subsequent performing more cycles [86]. In the current study, an aqueous mixture of (0.10 M NaOH + 1.20 M NaCl) was used to separate AR57/MB dyes after the NH_2-MIL-101(Cr) surface. Six rounds of the adsorption, desorption, and re-adsorption were examined, and the results are shown in Table 7. After six cycles the desorbtion is slowly reduced to 91.98 and 92.00% for AR57 and MB, respectively, subsequently at the beginning of the interaction between the AR57/MB dyes and NH_2-MIL-101(Cr) with 98.95% and 98.60% for AR57 and MB, respectively [87]. In particular, this minor reduction in the desorption percentage (≈6%) can be attributed to particles aggregating (blocking) of the active positions
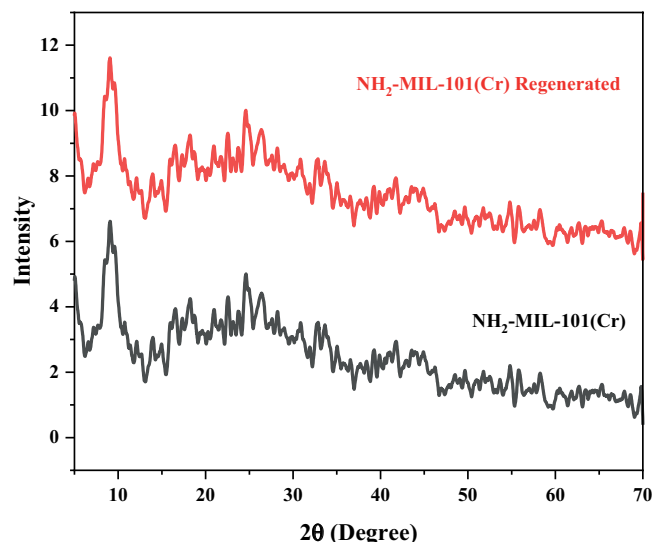
Fig. 20. X-ray diffraction spectra of NH_2-MIL-101(Cr) and regenerated NH_2-MIL-101(Cr).

Table 7
Adsorption, desorption, and re-adsorption of AR57 and MB dyes against NH_2-MIL-101(Cr) adsorbent surface after six cycles

Adsorption/ desorption cycle	q_e (adsorption) (mmol/g)		q_e (desorption) (mmol/g)		Desorp. (%)	
	AR57	MB	AR57	MB	AR57	MB
Cycle 1	1.718	1.716	1.700	1.692	98.95	98.60
Cycle 2	1.708	1.716	1.660	1.664	97.19	96.97
Cycle 3	1.708	1.698	1.640	1.621	96.02	95.47
Cycle 4	1.690	1.652	1.614	1.567	95.50	94.85
Cycle 5	1.653	1.621	1.541	1.502	93.22	92.66
Cycle 6	1.633	1.601	1.502	1.473	91.98	92.00

Electron density

Molecular electrostatic potential (MEP)

(a)

(b)

Fig. 19. Electron density of molecular electrostatic potential (MEP) of AR57 (a) and MB (b) used to map the total electron density surface.

happening the adsorbent surface (chemical reaction) [88]. Though, it is value importance that the sensibly rising NH_2-MIL-101(Cr) repeatability specifically indicated its cost-effective in treatment of water and wastewater facilities [68]. Following 6th cycle of testing, we used XRD to analyse the NH_2-MIL-101(Cr) samples and found that the crystallinity and structural were still present (Fig. 20). According to the result, NH_2-MIL-101(Cr) nanoparticles have a high reusability. By applying Eq. (18), the regeneration efficiency was considered.

$$\text{Regeneration efficiency}(\%)$$
$$= \frac{\begin{array}{c}\text{Total capacity for adsorption}\\\text{in the second run}\end{array}}{\begin{array}{c}\text{Total capacity for adsorption}\\\text{in the First run}\end{array}} \times 100 \quad (18)$$

4. Conclusions

This study presented NH_2-MIL-101(Cr), which was successfully manufactured by hydrothermal technique and characterized with XRD, SEM as determined average diameter of the adsorbent measured was ~68.50 nm, BET surface area of 1467.75 m^2/g, as well as a pore volume of 2.15 cm^3/g and a pore size of 2.90 nm. Research work was done to investigate the adsorptive removal of NH_2-MIL-101(Cr) against two main dyes (AR57 and MB) used as reference cases. The results showed that NH_2-MIL-101(Cr) has a high removal 1.75 mmol/g for AR57 and 1.72 mmol/g for MB at pH 3 and 9, respectively. Under optimal conditions, the adsorption kinetics fitted well pseudo-second-order. The adsorption isotherm data best fitted Langmuir and further supported by Dubinin–Radunkevich, Weber and Morris and Temkin. The thermodynamic parameters of NH_2-MIL-101(Cr) shown that the adsorption system was spontaneous and endothermic, confirming the chemisorption process. The produced NH_2-MIL-101(Cr) possibly reusable up to six cycles without losing its adsorption ability and simple to separate. Also, represented the suggested mechanism of interaction according to the DFT calculation as well as the active sites of both dyes.

Data availability statement

The corresponding author is willing to provide data that support the study's findings upon reasonable request.

Declaration of competing interest

No conflicts need be reported.

References

[1] M. Teotia, A. Mittal, R.K. Soni, Light-Mediated Thermoset Polymers, Materials for Biomedical Engineering, Elsevier, 2019, pp. 57–103.

[2] J. Mittal, Recent progress in the synthesis of layered double hydroxides and their application for the adsorptive removal of dyes: a review, J. Environ. Manage., 295 (2021) 113017.

[3] T.A. Altalhi, M.M. Ibrahim, G.A.M. Mersal, M.H.H. Mahmoud, T. Kumeria, M.G. El-Desouky, A.A. El-Bindary, M.A. El-Bindary, Adsorption of doxorubicin hydrochloride onto thermally treated green adsorbent: equilibrium, kinetic and thermodynamic studies, J. Mol. Struct., 1263 (2022) 133160.

[4] L. Qin, G. Zeng, C. Lai, D. Huang, P. Xu, C. Zhang, M. Cheng, X. Liu, S. Liu, B. Li, "Gold rush" in modern science: fabrication strategies and typical advanced applications of gold nanoparticles in sensing, Coord. Chem. Rev., 359 (2018) 1–31.

[5] C. Arora, S. Sonia, P. Bajpaib, J. Mittalc, A. Mariyam, Dye removal from waste water using metal organic frameworks, Manag. Contam. Emerg. Conc. Environ., 375 (2021).

[6] J. Mittal, Permissible synthetic food dyes in India, Resonance, 25 (2020) 567–577.

[7] J. Mittal, A. Mariyam, F. Sakina, R.T. Baker, A.K. Sharma, A. Mittal, Batch and bulk adsorptive removal of anionic dye using metal/halide-free ordered mesoporous carbon as adsorbent, J. Cleaner Prod., 321 (2021) 129060.

[8] J. Mittal, R. Ahmad, M.O. Ejaz, A. Mariyam, A. Mittal, A novel, eco-friendly bio-nanocomposite (Alg-Cst/Kal) for the adsorptive removal of crystal violet dye from its aqueous solutions, Int. J. Phytorem., 24 (2022) 796–807.

[9] M.G. El-Desouky, A. Shahat, A.A. El-Bindary, M.A. El-Bindary, Description, kinetic and equilibrium studies of the adsorption of carbon dioxide in mesoporous iron oxide nanospheres, Biointerf. Res. Appl. Chem., 12 (2022) 1022–1038.

[10] M.G. El-Desouky, M.A. Khalil, A.A. El-Bindary, M.A. El-Bindary, Biological, biochemical and thermochemical techniques for biofuel production: an updated review, Biointerf. Res. Appl. Chem., 12 (2022) 3034–3054.

[11] H.-Y. Guan, R.J. LeBlanc, S.-Y. Xie, Y. Yue, Recent progress in the syntheses of mesoporous metal–organic framework materials, Coord. Chem. Rev., 369 (2018) 76–90.

[12] M. Feng, P. Zhang, H.-C. Zhou, V.K. Sharma, Water-stable metal-organic frameworks for aqueous removal of heavy metals and radionuclides: a review, Chemosphere, 209 (2018) 783–800.

[13] A.A. El-Bindary, M.G. El-Desouky, M.A.M. El-Afify, Thermal and spectroscopic studies of some prepared metal complexes and investigation of their potential anticancer and antiviral drug activity against SARS-CoV-2 by molecular docking simulation, Biointerf. Res. Appl. Chem., 12 (2022) 1053–1075.

[14] A. Mariyam, J. Mittal, F. Sakina, R.T. Baker, A.K. Sharma, A. Mittal, Efficient batch and fixed-bed sequestration of a basic dye using a novel variant of ordered mesoporous carbon as adsorbent, Arabian J. Chem., 14 (2021) 103186.

[15] J. Mittal, P. Ahmad, A. Mittal, Kahwa tea (*Camellia sinensis*) carbon—a novel and green low-cost adsorbent for the sequestration of titan yellow dye from its aqueous solutions, Desal. Water Treat., 227 (2021) 404–411.

[16] A. Patel, S. Soni, J. Mittal, A. Mittal, C. Arora, Sequestration of crystal violet from aqueous solution using ash of black turmeric rhizome, Desal. Water Treat., 220 (2021) 342–352.

[17] J. Mittal, R. Ahmad, A. Mariyam, V. Gupta, A. Mittal, Expeditious and enhanced sequestration of heavy metal ions from aqueous environment by papaya peel carbon: a green and low-cost adsorbent, Desal. Water Treat., 210 (2021) 365–376.

[18] S. Soni, P. Bajpai, J. Mittal, C. Arora, Utilisation of cobalt doped Iron based MOF for enhanced removal and recovery of methylene blue dye from waste water, J. Mol. Liq., 314 (2020) 113642.

[19] N. Ranga, E. Poonia, S. Jakhar, A.K. Sharma, A. Kumar, S. Devi, S. Duhan, Enhanced antimicrobial properties of bioactive glass using strontium and silver oxide nanocomposites, J. Asian Ceram. Soc., 7 (2019) 75–81.

[20] A.K. Sharma, Y. Sharma, p-toluene sulfonic acid doped polyaniline carbon nanotube composites: synthesis via different routes and modified properties, J. Electrochem. Sci. Eng., 3 (2013) 47–56.

[21] D. Bhatia, D. Datta, A. Joshi, S. Gupta, Y. Gote, Adsorption of isonicotinic acid from aqueous solution using multi-walled carbon nanotubes/Fe_3O_4, J. Mol. Liq., 276 (2019) 163–169.

[22] L. Zhang, J. Wang, T. Du, W. Zhang, W. Zhu, C. Yang, T. Yue, J. Sun, T. Li, J. Wang, NH2-MIL-53 (Al) metal–organic

framework as the smart platform for simultaneous high-performance detection and removal of Hg²⁺, Inorg. Chem., 58 (2019) 12573–12581.

[23] A. Mariyam, J. Mittal, F. Sakina, R.T. Baker, A.K. Sharma, Fixed-bed adsorption of the dye Chrysoidine R on ordered mesoporous carbon, Desal. Water Treat., (2021).

[24] M.G. El-Desouky, N. Hassan, A. Shahat, A. El-Didamony, A.A. El-Bindary, Synthesis and characterization of porous magnetite nanosphere iron oxide as a novel adsorbent of anionic dyes removal from aqueous solution, Biointerf. Res. Appl. Chem., 11 (2021) 13377–13401.

[25] N. Hassan, A. Shahat, A. El-Didamony, M.G. El-Desouky, A.A. El-Bindary, Mesoporous iron oxide nano spheres for capturing organic dyes from water sources, J. Mol. Struct., 1217 (2020) 128361.

[26] N. Hassan, A. Shahat, I.M. El-Deen, M.A.M. El-Afify, M.A. El-Bindary, Synthesis and characterization of NH2-MIL-88 (Fe) for efficient adsorption of dyes, J. Mol. Struct., 1258 (2022) 132662.

[27] N. Hassan, A. Shahat, A. El-Didamony, M.G. El-Desouky, A.A. El-Bindary, Equilibrium, kinetic and thermodynamic studies of adsorption of cationic dyes from aqueous solution using ZIF-8, Moroc. J. Chem., 8 (2020) 624–635.

[28] S. Soni, P.K. Bajpai, D. Bharti, J. Mittal, C. Arora, Removal of crystal violet from aqueous solution using iron based metal organic framework, Desal. Water Treat., 205 (2020) 386–399.

[29] N. Hassan, A. Shahat, A. El-Didamony, M.G. El-Desouky, A.A. El-Bindary, Synthesis and characterization of ZnO nanoparticles via zeolitic imidazolate framework-8 and its application for removal of dyes, J. Mol. Struct., 1210 (2020) 128029.

[30] V.K. Gupta, S. Agarwal, R. Ahmad, A. Mirza, J. Mittal, Sequestration of toxic Congo red dye from aqueous solution using ecofriendly guar gum/activated carbon nanocomposite, Int. J. Biol. Macromol., 158 (2020) 1310–1318.

[31] K.Z. Elwakeel, A.A. El-Bindary, A. Ismail, A.M. Morshidy, Magnetic chitosan grafted with polymerized thiourea for remazol brilliant blue R recovery: effects of uptake conditions, J. Dispersion Sci. Technol., 38 (2017) 943–952.

[32] M.A. El-Bindary, M.G. El-Desouky, A.A. El-Bindary, Adsorption of industrial dye from aqueous solutions onto thermally treated green adsorbent: a complete batch system evaluation, J. Mol. Liq., 346 (2022) 117082.

[33] R. Jain, P. Sharma, S. Sikarwar, J. Mittal, D. Pathak, Adsorption kinetics and thermodynamics of hazardous dye Tropaeoline 000 unto Aeroxide Alu C (Nano alumina): a non-carbon adsorbent, Desal. Water Treat., 52 (2014) 7776–7783.

[34] A. Mariyam, J. Mittal, F. Sakina, R.T. Baker, A.K. Sharma, Adsorption behaviour of Chrysoidine R dye on a metal/halide-free variant of ordered mesoporous carbon, Desal. Water Treat. Sci. Eng., 223 (2021) 425–433.

[35] A.S. Al-Wasidi, I.I.S. AlZahrani, H.I. Thawibaraka, A.M. Naglah, M.G. El-Desouky, M.A. El-Bindary, Adsorption studies of carbon dioxide and anionic dye on green adsorbent, J. Mol. Struct., 1250 (2022) 131736.

[36] A.S. Al-Wasidi, I.I.S. AlZahrani, A.M. Naglah, M.G. El-Desouky, M.A. Khalil, A.A. El-Bindary, M.A. El-Bindary, Effective removal of methylene blue from aqueous solution using metal-organic framework; modelling analysis, statistical physics treatment and DFT calculations, ChemistrySelect, 6 (2021) 11431–11447.

[37] P. Saharan, V. Kumar, J. Mittal, V. Sharma, A.K. Sharma, Efficient ultrasonic assisted adsorption of organic pollutants employing bimetallic-carbon nanocomposites, Sep. Sci. Technol., 56 (2021) 2895–2908.

[38] M.I. El-Khaiary, G.F. Malash, Common data analysis errors in batch adsorption studies, Hydrometallurgy, 105 (2011) 314–320.

[39] H. Naeem, H.N. Bhatti, S. Sadaf, M. Iqbal, Uranium remediation using modified *Vigna radiata* waste biomass, Appl. Radiat. Isot., 123 (2017) 94–101.

[40] S. Shoukat, H.N. Bhatti, M. Iqbal, S. Noreen, Mango stone biocomposite preparation and application for crystal violet adsorption: a mechanistic study, Microporous Mesoporous Mater., 239 (2017) 180–189.

[41] N. Tahir, H.N. Bhatti, M. Iqbal, S. Noreen, Biopolymers composites with peanut hull waste biomass and application for Crystal violet adsorption, Int. J. Biol. Macromol., 94 (2017) 210–220.

[42] M.G. El-Desouky, A.A. El-Bindary, M.A. El-Bindary, Low-temperature adsorption study of carbon dioxide on porous magnetite nanospheres iron oxide, Biointerf. Res. Appl. Chem., 12 (2022) 6252–6268.

[43] K.S. Hameed, P. Muthirulan, M.M. Sundaram, Adsorption of chromotrope dye onto activated carbons obtained from the seeds of various plants: equilibrium and kinetics studies, Arab. J. Chem., 10 (2017) S2225–S2233.

[44] S. Wong, N.A.N. Yac'cob, N. Ngadi, O. Hassan, I.M. Inuwa, From pollutant to solution of wastewater pollution: Synthesis of activated carbon from textile sludge for dye adsorption, Chin. J. Chem. Eng., 26 (2018) 870–878.

[45] H.N. Tran, E.C. Lima, R.-S. Juang, J.-C. Bollinger, H.-P. Chao, Thermodynamic parameters of liquid–phase adsorption process calculated from different equilibrium constants related to adsorption isotherms: a comparison study, J. Environ. Chem. Eng., 9 (2021) 106674.

[46] K.Y. Foo, B.H. Hameed, Insights into the modeling of adsorption isotherm systems, Chem. Eng. J., 156 (2010) 2–10.

[47] M. Liu, J. Wang, Q. Yang, N. Hu, W. Zhang, W. Zhu, R. Wang, Y. Suo, J. Wang, Patulin removal from apple juice using a novel cysteine-functionalized metal-organic framework adsorbent, Food Chem., 270 (2019) 1–9.

[48] I. Langmuir, The constitution and fundamental properties of solids and liquids. II. Liquids, J. Am. Chem. Soc., 39 (1917) 1848–1906.

[49] I. Langmuir, The adsorption of gases on plane surfaces of glass, mica and platinum, J. Am. Chem. Soc., 40 (1918) 1361–1403.

[50] H. Freundlich, W. Heller, The adsorption of cis-and trans-azobenzene, J. Am. Chem. Soc., 61 (1939) 2228–2230.

[51] M. Dubinin, Sorbtsiya I Struktura Aktivnykh Uglei 1. Issledovanie Adsorbtsii Organicheskikh Parov, Zh. Fiz. Khim., 21 (1947) 1351–1362.

[52] Y. Qiu, H. Guo, C. Guo, J. Zheng, T. Yue, Y. Yuan, One-step preparation of nano-Fe₃O₄ modified inactivated yeast for the adsorption of patulin, Food Control, 86 (2018) 310–318.

[53] S.-W. Lv, J.-M. Liu, C.-Y. Li, N. Zhao, Z.-H. Wang, S. Wang, A novel and universal metal-organic frameworks sensing platform for selective detection and efficient removal of heavy metal ions, Chem. Eng. J., 375 (2019) 122111.

[54] S.A. El-Safty, A. Shahat, M. Ismael, Mesoporous aluminosilica monoliths for the adsorptive removal of small organic pollutants, J. Hazard. Mater., 201 (2012) 23–32.

[55] S. El-Safty, A. Shahat, K. Ogawa, T. Hanaoka, Highly ordered, thermally/hydrothermally stable cubic Ia3d aluminosilica monoliths with low silica in frameworks, Microporous Mesoporous Mater., 138 (2011) 51–62.

[56] A.M. Aldawsari, I.H. Alsohaimi, H.M. Hassan, M.R. Berber, Z.E. Abdalla, I. Hassan, E.A.M. Saleh, B.H. Hameed, Activated carbon/MOFs composite: AC/NH2-MIL-101(Cr), synthesis and application in high performance adsorption of p-nitrophenol, J. Saudi Chem. Soc., 24 (2020) 693–703.

[57] S. Lagergren, About the theory of so-called adsorption of soluble substances, J. Sven. Vetenskapsakad. Handingarl., 24 (1898) 1–39.

[58] Y.-S. Ho, G. McKay, Sorption of dye from aqueous solution by peat, Chem. Eng. J., 70 (1998) 115–124.

[59] J. Zeldowitsch, Über den mechanismus der katalytischen oxydation von CO an MnO₂, Acta physicochim. URSS, 1 (1934) 364–449.

[60] H.N. Tran, S.-J. You, A. Hosseini-Bandegharaei, H.-P. Chao, Mistakes and inconsistencies regarding adsorption of contaminants from aqueous solutions: a critical review, Water Res., 120 (2017) 88–116.

[61] K. Tan, B. Hameed, Insight into the adsorption kinetics models for the removal of contaminants from aqueous solutions, J. Taiwan Inst. Chem. Eng., 74 (2017) 25–48.

[62] B. Hameed, R. Krishni, S. Sata, A novel agricultural waste adsorbent for the removal of cationic dye from aqueous solutions, J. Hazard. Mater., 162 (2009) 305–311.

[63] H.A. Kiwaan, F.Sh. Mohamed, A.A. El-Bindary, N.A. El-Ghamaz, H.R. Abo-Yassin, M.A. El-Bindary, Synthesis, identification and application of metal organic framework for removal of industrial cationic dyes, J. Mol. Liq., 342 (2021) 117435.

[64] K.Z. Elwakeel, A. Shahat, A.S. Al-Bogami, B. Wijesiri, A. Goonetilleke, The synergistic effect of ultrasound power and magnetite incorporation on the sorption/desorption behavior of Cr(VI) and As(V) oxoanions in an aqueous system, J. Colloid Interface Sci., 569 (2020) 76–88.

[65] E.C. Lima, A.A. Gomes, H.N. Tran, Comparison of the nonlinear and linear forms of the van't Hoff equation for calculation of adsorption thermodynamic parameters ($\Delta S°$ and $\Delta H°$), J. Mol. Liq., 311 (2020) 113315.

[66] M.A. Karimi, H. Masrouri, M.A. Mirbagheri, S. Andishgar, T. Pourshamsi, Synthesis of a new magnetic metal–organic framework nanocomposite and its application in methylene blue removal from aqueous solution, J. Chin. Chem. Soc., 65 (2018) 1229–1238.

[67] M.E. Gonzalez-Lopez, C.M. Laureano-Anzaldo, A.A. Perez-Fonseca, M. Arellano, J.R. Robledo-Ortiz, A critical overview of adsorption models linearization: methodological and statistical inconsistencies, Sep. Purif. Rev., 51 (2022) 358–372.

[68] A.M. Elgarahy, A. Akhdhar, A.S. Al-Bogami, K.Z. Elwakeel, Magnetically separable solid phase extractor for static anionic dyes adsorption from aqueous solutions, Surf. Interfaces, 30 (2022) 101962.

[69] C.E. de Farias Silva, B.M.V. da Gama, A.H. da Silva Gonçalves, J.A. Medeiros, A.K. de Souza Abud, Basic-dye adsorption in albedo residue: effect of pH, contact time, temperature, dye concentration, biomass dosage, rotation and ionic strength, J. King Saud Univ. Eng. Sci., 32 (2020) 351–359.

[70] R. Lafi, L. Abdellaoui, I. Montasser, A. Hafiane, Removal of methyl orange from aqueous solution onto modified extracted cellulose from *Stipa Tenacissima* L, Int. J. Environ. Anal. Chem., (2020) 1–17.

[71] K.Z. Elwakeel, A. Shahat, Z.A. Khan, W. Alshitari, E. Guibal, Magnetic metal oxide-organic framework material for ultrasonic-assisted sorption of titan yellow and rose bengal from aqueous solutions, Chem. Eng. J., 392 (2020) 123635.

[72] A. Özcan, A.S. Özcan, Adsorption of Acid Red 57 from aqueous solutions onto surfactant-modified sepiolite, J. Hazard Mater., 125 (2005) 252–259.

[73] A.S. Özcan, Ş. Tetik, A. Özcan, Adsorption of acid dyes from aqueous solutions onto sepiolite, J. Sep. Sci. Technol., 39 (2005) 301–320.

[74] D. Karataş, D. Senol-Arslan, O. Ozdemir, Experimental and atomic modeling of the adsorption of acid azo dye 57 to sepiolite, J. Clay Miner., 66 (2018) 426–437.

[75] A.S. Özcan, A. Özcan, Adsorption of acid dyes from aqueous solutions onto acid-activated bentonite, J. Colloid Interface Sci., 276 (2004) 39–46.

[76] M.R. Malekbala, S. Hosseini, S. Masoudi Soltani, R. Malekbala, T.S. Choong, F. Eghbali Babadi, Development, application,

and evaluation of artificial neural network in investigating the removal efficiency of Acid Red 57 by synthesized mesoporous carbon-coated monoliths, Desalination, 56 (2015) 2246–2257.

[77] B. Hameed, A. Ahmad, K. Latiff, Adsorption of basic dye (methylene blue) onto activated carbon prepared from rattan sawdust, Dyes Pigm., 75 (2007) 143–149.

[78] E.O. Akperov, O.H. Akperov, The wastage of the cotton stalks (Gossypium hirsutum L.) as low-cost adsorbent for removal of the Basic Green 5 dye from aqueous solutions, Appl. Water Sci., 9 (2019) 1–9.

[79] C. Arora, S. Soni, S. Sahu, J. Mittal, P. Kumar, P. Bajpai, Iron based metal organic framework for efficient removal of methylene blue dye from industrial waste, J. Mol. Liq., 284 (2019) 343–352.

[80] J. Hu, W. Dai, X. Yan, Comparison study on the adsorption performance of methylene blue and Congo red on Cu-BTC, Desal. Water Treat., 57 (2016) 4081–4089.

[81] L. Li, X.L. Liu, H.Y. Geng, B. Hu, G.W. Song, Z.S. Xu, A MOF/ graphite oxide hybrid (MOF: HKUST-1) material for the adsorption of methylene blue from aqueous solution, J. Mater. Chem., 1 (2013) 10292–10299.

[82] H.A. Kiwaan, F.Sh. Mohamed, N.A. El-Ghamaz, N.M. Beshry, A.A. El-Bindary, Experimental and electrical studies of Na-X zeolite for the adsorption of different dyes, J. Mol. Liq., 332 (2021) 115877.

[83] T.J.M. Fraga, M.N. Carvalho, D.M.d.S.M. Fraga, M.d.C.L. da Silva, J.M. Ferreira, M.A. da Motta Sobrinho, Treated residue from aluminium lamination as adsorbent of toxic reactive dyes–a kinetic, equilibrium and thermodynamic study, Environ. Technol., 41 (2020) 669–681.

[84] H. Lgaz, R. Salghi, S. Jodeh, Y. Ramli, M. Larouj, K. Toumiat, W. Jodeh, Understanding the adsorption of quinoxaline derivatives as corrosion inhibitors for mild steel in acidic medium: experimental, theoretical and molecular dynamic simulation studies, J. Steel Struct. Constr., 2 (2016) 2472-0437.100011.

[85] A. Nakhli, M. Bergaoui, K.H. Toumi, M. Khalfaoui, Y. Benguerba, M. Balsamo, F.E. Soetaredjo, S. Ismadji, B. Ernst, A. Erto, Molecular insights through computational modeling of methylene blue adsorption onto low-cost adsorbents derived from natural materials: a multi-model's approach, Comput. Chem. Eng., 140 (2020) 106965.

[86] G.A. Al-Hazmi, K.S. AbouMelha, M.G. El-Desouky, A.A. El-Bindary, Effective adsorption of doxorubicin hydro-chloride on zirconium metal-organic framework: equilibrium, kinetic and thermodynamic studies, J. Mol. Struct., 1258 (2022) 132679.

[87] M.A. El-Bindary, M.G. El-Desouky, A.A. El-Bindary, Metal-organic frameworks encapsulated with an anticancer compound as drug delivery system: synthesis, characterization, antioxidant, anticancer, antibacterial, and molecular docking investigation, Appl. Organomet. Chem., 36 (2022) e6660.

[88] H.A. Kiwaan, F.Sh. Mohamed, N.A. El-Ghamaz, N.M. Beshry, A.A. El-Bindary, Experimental and electrical studies of zeolitic imidazolate framework-8 for the adsorption of different dyes, J. Mol. Liq., 338 (2021) 116670.